

A fast and precise way to calculate the posterior for the local non-Gaussianity parameter f_{nl} from Cosmic Microwave Background observations

Sebastian Dorn^{*,1,2}, Niels Oppermann¹, Rishi Khatri¹, Marco Selig¹, and Torsten A. Enßlin¹

¹ *Max-Planck-Institut für Astrophysik, Karl-Schwarzschild-Str. 1, 85748 Garching, Germany*

² *Technische Universität München, Arcisstraße 21, 80333 München, Germany*

(Dated: July 16, 2013)

Abstract. We present an approximate calculation of the full Bayesian posterior probability distribution for the local non-Gaussianity parameter f_{nl} from observations of Cosmic Microwave Background anisotropies within the framework of information field theory. The approximation that we introduce allows us to dispense with numerically expensive sampling techniques. We use a novel posterior validation method (DIP-test) in cosmology to test the precision of our method. It transfers inaccuracies of the calculated posterior into deviations from a uniform distribution for a specially constructed test quantity. For this procedure we study toy-cases that use one- and two-dimensional flat skies, as well as the full spherical sky. We find that we are able to calculate the posterior precisely under a flat-sky approximation, albeit not in the spherical case. We argue that this is most likely due to an insufficient precision of the used numerical implementation of the spherical harmonic transform, which might affect other non-Gaussianity estimators as well. Furthermore, we present how a non-linear reconstruction of the primordial gravitational potential on the full spherical sky can be obtained in principle. Using the flat-sky approximation, we find deviations for the posterior of f_{nl} from a Gaussian shape that become more significant for larger values of the underlying true f_{nl} . We also perform a comparison to the well-known estimator of Komatsu et al. (2005) and finally derive the posterior for the local non-Gaussianity parameter g_{nl} as an example of how to extend the introduced formalism to higher orders of non-Gaussianity.

Subject headings: Cosmic Microwave Background - cosmology - information field theory - critical test - Bayesian inference.

I. INTRODUCTION

The statistics of the observed temperature fluctuations of the Cosmic Microwave Background (CMB) radiation have opened a window into the physics of the very early Universe [1–3]. Of special importance due to its relative simplicity and far-reaching implications is the study of local non-Gaussianities in the temperature distribution (e.g. [4]). We present a novel, fast, and accurate way of characterizing the level of these non-Gaussianities from CMB observations.

The fluctuations in the temperature of the CMB radiation include perturbations of the primordial gravitational potential φ during inflation. Their statistics can be described well by a Gaussian distribution, except for small deviations [1, 5–7]. The strength of these deviations depends on the exact mechanism behind inflation and can in many cases, e.g. multi-field inflation models [8], be parametrized by a local non-Gaussianity parameter f_{nl} [9],

$$\varphi(x) = \phi(x) + f_{\text{nl}}(\phi^2(x) - \widehat{\Phi}) + \mathcal{O}(\phi^3), \quad (1)$$

where ϕ is a Gaussian field with covariance Φ , $\widehat{\Phi} = \langle \phi^2(x) \rangle_{(\phi|\Phi)}$ denotes the local variance, i.e., the diagonal of Φ in position space assumed here to be position-independent, and the f_{nl} -parameter is a measure for the

degree of non-Gaussianity. While standard single-field slow-roll inflation theories [10] predict small values of $f_{\text{nl}} \ll 1$, multi-field inflation theories [8] predict larger f_{nl} -values up to the order of $\mathcal{O}(10^2)$ [4]. Therefore, any detection or upper limit of f_{nl} rules out some inflation models and might enable us to select between the remaining ones. Recent data from the *Planck* satellite constrain the non-Gaussianity to $f_{\text{nl}} = 2.7 \pm 5.8$ (68% CL statistical) [3].

A non-zero value of f_{nl} causes a correlation between the strength of small-scale anisotropies and large-scale fluctuations. In the case of positive f_{nl} the probability density function (PDF) of the CMB temperature anisotropies is negatively skewed whereas a negative f_{nl} provides a positively skewed PDF [11]. Negatively (positively) skewed means that the left (right) tail of the PDF is longer.

A common method to determine this skewness and thus f_{nl} is to investigate the bispectrum of the CMB [12]. A few authors (e.g. [13–15]) have recognized that the uncertainty of f_{nl} depends on the data realization. Bayesian approaches, which were developed over the last few years as well (e.g. [15–18]), provide a comfortable way to cope with uncertainties. Most of these approaches, however, require computationally expensive calculations like Monte Carlo sampling. The determination of the exact shape of the tails of the PDF is especially expensive when using such techniques.

In this work we introduce a precise Bayesian approach to determine the posterior density function for the local non-Gaussianity parameter without sampling over the data space as opposed to traditional estimators (e.g. the

*sdorn@mpa-garching.mpg.de

Komatsu-Spergel-Wandelt (KSW) -estimator [12]). This is made possible by the use of an analytic approximation in the framework of information field theory [17].

We provide a validation of the posterior (DIP-test [19]) calculated in this way to show that the precision is not significantly reduced by our approximation.

The remainder of this paper is organized as follows. In Sec. II, we introduce our assumptions about the relationship between the observed data and the primordial gravitational field and derive the approximate form of the posterior probability distribution for the local non-Gaussianity parameter. In Sec. III, we validate the accuracy of the calculated posterior and apply it in flat sky and all-sky test-cases. A non-linear reconstruction of the primordial potential, a comparison to the *KSW*-estimator, and the investigation of the shape of the posterior are also shown in this section. In Sec. IV we show how the formalism can be extended to cope with deviations from Gaussianity of higher order. We summarize our findings in Sec. V.

II. THE BAYESIAN f_{nl} -POSTERIOR

A. Data model

To determine the level of non-Gaussianity of the primordial gravitational potential φ , one has to analyze a data set d that is sensitive to φ . Here we focus on CMB temperature observations. We consider this data set to be in the form $d = (d_1, d_2, \dots, d_m)^T \in \mathbb{R}^m$, where $m \in \mathbb{N}$. These data depend linearly on φ and on additive noise $n = (n_1, n_2, \dots, n_m)^T$,

$$d := \frac{\delta T_{\text{obs}}}{T_{\text{CMB}}} = R\varphi + n, \quad (2)$$

where R denotes the *signal response operator*. The primordial gravitational potential is a continuous quantity, $\varphi : \mathcal{U} \rightarrow \mathbb{R}$, i.e., a scalar field. \mathcal{U} is the manifold on which φ is defined, e.g. the three-dimensional position space or the sphere \mathcal{S}^2 . The signal response contains all instrumental and measurement effects on the primordial gravitational potential, e.g. a convolution of φ with a telescope beam and a transfer function describing the physics at recombination. We will ignore the first effect and use, for simplicity, the *Sachs-Wolfe* transfer function [20, 21], $\Delta T/T = -\varphi/3$, which is valid on large scales. In this case \mathcal{U} is the surface of last scattering, isomorphic to \mathcal{S}^2 . However, our formalism is generic and we also demonstrate in Sec. III.D that it can cope with non-local responses. Henceforth we will follow the notation of information field theory [17].

As a first step, we assume that the data d are given and we want to reconstruct φ from them. To figure out which configurations for the primordial gravitational potential φ are likely given these experimentally determined quantities d , one has to study the posterior probability

distribution $P(\varphi|d)$. We can rewrite the posterior probability $P(\varphi|d)$ by defining an *information Hamiltonian* H [17] via Bayes' Theorem [22],

$$P(\varphi|d) = \frac{P(d|\varphi)P(\varphi)}{P(d)} =: \frac{1}{Z} e^{-H(d,\varphi)}, \quad (3)$$

where $H(d, \varphi) = -\ln(P(d|\varphi)P(\varphi))$ and the *partition function* $Z = P(d)$ was introduced.

Throughout the paper we assume Gaussian noise,

$$P(n|N) = \frac{1}{|2\pi N|^{1/2}} \exp\left(-\frac{1}{2}n^\dagger N^{-1}n\right) =: \mathcal{G}(n, N), \quad (4)$$

where $N = \langle nn^\dagger \rangle_{(n|N)}$ is the noise covariance matrix, \dagger a transposition and complex conjugation, the latter denoted by $*$, and

$$n^\dagger N^{-1}n = \sum_k \sum_l n_k^* (N^{-1})_{kl} n_l. \quad (5)$$

For the Gaussian field ϕ , the exponent of the probability density distribution function $P(\phi) = \mathcal{G}(\phi, \Phi)$ can be written as

$$\phi^\dagger \Phi^{-1} \phi = \int_{\mathcal{U}} du \int_{\mathcal{U}} dv \phi^*(u) \Phi^{-1}(u, v) \phi(v), \quad (6)$$

with $\Phi = \langle \phi \phi^\dagger \rangle_{(\phi|\Phi)}$ the covariance operator of the Gaussian field ϕ .

B. Approximation of the f_{nl} -posterior

Posterior setup. Assuming Eqs. (1) and (2) for the data yields

$$d = R\left(\phi + f_{\text{nl}}\left(\phi^2 - \widehat{\Phi}\right)\right) + n. \quad (7)$$

The response R , which can be calculated theoretically [23–25], transforms the gravitational potential into a temperature map. Assuming a fixed value of f_{nl} , the information Hamiltonian becomes [17]

$$\begin{aligned} H(d, \phi|f) &= -\ln(P(d, \phi|f)) = -\ln(P(d|\phi, f)P(\phi|f)) \\ &= -\ln(\mathcal{G}(d - R(\phi + f(\phi^2 - \widehat{\Phi})), N)\mathcal{G}(\phi, \Phi)) \\ &= H_0 + \frac{1}{2}\phi^\dagger D^{-1}\phi - j^\dagger \phi + \sum_{n=0}^4 \frac{1}{n!} \Lambda^{(n)}[\phi, \dots, \phi], \end{aligned} \quad (8)$$

with the abbreviations

$$\begin{aligned}
f &= f_{\text{nl}}, \\
M &= R^\dagger N^{-1} R, \\
H_0 &= \frac{1}{2} \ln |2\pi\Phi| + \frac{1}{2} \ln |2\pi N| + \frac{1}{2} d^\dagger N^{-1} d, \\
D^{-1} &= \Phi^{-1} + M, \\
j &= R^\dagger N^{-1} d, \\
\Lambda^{(0)} &= j^\dagger (f\widehat{\Phi}) + \frac{1}{2} (f\widehat{\Phi})^\dagger M (f\widehat{\Phi}), \\
\Lambda^{(1)} &= -(f\widehat{\Phi})^\dagger M, \\
\Lambda^{(2)} &= -2f\widehat{j}' \text{ with } j' = j - \Lambda^{(1)\dagger}, \\
\Lambda^{(3)} &= (M_{xy} f_y \delta_{yz} + 5 \text{ perturbations}), \\
\Lambda^{(4)} &= \frac{1}{2} (f_x \delta_{xy} M_{yz} \delta_{zu} f_u + 23 \text{ perturbations}).
\end{aligned} \tag{9}$$

Here and in the following the hat on the vector fj' denotes a diagonal matrix, \widehat{fj}' , whose entries are given by $\widehat{fj}'_{xx} = f_x j'_x$ and $\Lambda^{(n)}[\phi, \dots, \phi]$ denotes a complete contraction between the rank- n tensor $\Lambda^{(n)}$ and the n fields ϕ . In the case of a non-diagonal response or noise covariance the interactions $\Lambda^{(n)}$ are non-local. Eq. (9) permits to consider values of f_{nl} that vary from location to location, as noted in [17]. However, we want to concentrate on a single value of f_{nl} .

If we consider large scales, dominated by the Sachs-Wolfe effect [20], a local approximation exists, in which the response and the noise covariance are diagonal in position space [17, 21]¹ with

$$\begin{aligned}
N_{xy} &= \sigma_n^2 \delta_{xy}, \\
R(x, y) &= -\frac{1}{3} \delta(x - y).
\end{aligned} \tag{10}$$

Posterior approximation. We aim to determine the PDF for the f_{nl} -parameter and thus are interested in

$$\begin{aligned}
P(f|d) &\propto P(d|f)P(f) \\
&\propto \int \mathcal{D}\phi P(d, \phi|f) = \int \mathcal{D}\phi \exp(-H(d, \phi|f)),
\end{aligned} \tag{11}$$

where we have assumed that $P(f) = \text{const}$ for simplicity. However, we are not able to perform the path integration because the Hamiltonian is not quadratic in the field ϕ .

An expansion in Feynman diagrams had therefore been proposed in [17]. Here, the central idea to circumvent this problem is to use a saddle point approximation by performing a Taylor expansion of the Hamiltonian up to the second order in ϕ around its minimum. This is possible because $|\phi| \sim \mathcal{O}(10^{-5})$ provides us with a small parameter and $P(\phi \approx 1)$ is negligibly small. To calculate this expansion we need the first and second functional derivatives of $H(d, \phi|f)$ with respect to ϕ . The minimum m is given by

$$\begin{aligned}
0 &= \frac{\delta H(d, \phi|f)}{\delta \phi} \Big|_{\phi=m} = (D^{-1} + \Lambda^{(2)})\phi - j + \left(\Lambda^{(1)}\right)^\dagger \\
&\quad + \frac{1}{3!} \frac{\delta}{\delta \phi} \Lambda^{(3)}[\phi, \phi, \phi] + \frac{1}{4!} \frac{\delta}{\delta \phi} \Lambda^{(4)}[\phi, \phi, \phi, \phi] \Big|_{\phi=m}.
\end{aligned} \tag{12}$$

Performing these derivatives yields (see (A1)-(A4))

$$\begin{aligned}
0 &= (D^{-1} + \Lambda^{(2)})m - j + \left(\Lambda^{(1)}\right)^\dagger \\
&\quad + \frac{1}{3!} (6fMm^2 + 12fm \star Mm) + \frac{1}{4!} (48f^2m \star Mm^2)
\end{aligned} \tag{13}$$

and the Hessian

$$\begin{aligned}
D_{d,f}^{-1} &:= \frac{\delta^2 H(d, \phi|f)}{\delta \phi^2} \Big|_{\phi=m} = D^{-1} + \Lambda^{(2)} \\
&\quad + (4fm \star M + 2f\widehat{Mm}) + (4f^2m^2 \star M + 2f^2\widehat{Mm^2}).
\end{aligned} \tag{14}$$

The \star denotes a pixel by pixel multiplication, e.g. $\phi_x^2 = (\phi \star \phi)_x := \phi_x \phi_x$, i.e., $\phi \star \phi$ is still a field and not a scalar. In the large-scale approximation, Eq. (10), where the response and the noise covariance matrix are diagonal, these equations simplify:

minimum:

$$0 = (D^{-1} + \lambda^{(2)})m - j + \lambda^{(1)} + \frac{1}{2}\lambda^{(3)}m^2 + \frac{1}{6}\lambda^{(4)}m^3$$

Hessian:

$$D_{d,f}^{-1} = D^{-1} + \lambda^{(2)} + \widehat{\lambda^{(3)}m} + \frac{1}{2}\widehat{\lambda^{(4)}m^2}. \tag{15}$$

$\lambda^{(1)}, \dots, \lambda^{(4)}$ are diagonal matrices arising from $\Lambda^{(1)}, \dots, \Lambda^{(4)}$ by replacing M_{xy} with $\sigma_n^{-2}\delta(x-y)/9$.

In our saddle point approximation the Hamiltonian therefore has the form

$$\begin{aligned}
H(d, \phi|f) &= H(d, m|f) + \frac{1}{2}(\phi - m)^\dagger D_{d,f}^{-1}(\phi - m) \\
&\quad + \mathcal{O}((\phi - m)^3),
\end{aligned} \tag{16}$$

¹ Note that in [17] the response is falsely assumed to be $R = -3$. Therefore, the following equations on page 26 of [17] have to be changed to $M_{xy} = \sigma_n^{-2}(x)\delta(x-y)/9$, $D^{-1} = \Phi^{-1} + \widehat{\sigma_n^{-2}}/9$, $j' = \frac{1}{3}(\frac{1}{3}f\widehat{\Phi} - d)/\sigma_n^2$, $\lambda_0 = \frac{1}{3}(\widehat{\Phi}\sigma_n^2)^\dagger(\frac{1}{6}f^2\widehat{\Phi}) - fd$, $\lambda_3 = \frac{2f}{3\sigma_n^2}$, and $\lambda_4 = \frac{4f^2}{3\sigma_n^2}$, where we have used that $R = -1/3$.

where we ignore third and fourth order terms in $(\phi - m)$. We are now able to perform the ϕ -marginalization,

$$\begin{aligned}
P(f|d) &\propto \int \mathcal{D}\phi \exp(-H(d, \phi|f)) \\
&\approx \int \mathcal{D}(\phi - m) \left| \frac{\delta(\phi - m)}{\delta\phi} \right|^{-1} \\
&\quad \times \exp\left(-H(d, m|f) - \frac{1}{2}(\phi - m)^\dagger D_{d,f}^{-1}(\phi - m)\right) \\
&= |2\pi D_{d,f}|^{\frac{1}{2}} \exp(-H(d, m|f)).
\end{aligned} \tag{17}$$

In this formula appears the f_{nl} -dependent determinant of the inverse Hessian, whose calculation is simplified by the following reformulation:

$$\begin{aligned}
|2\pi D_{d,f}|^{\frac{1}{2}} &= \exp\left(-\frac{1}{2} \ln |2\pi D_{d,f}|^{-1}\right) \\
&= \exp\left(-\frac{1}{2} \text{tr} \left[\ln \left(\frac{1}{2\pi} D_{d,f}^{-1} \right) \right]\right)
\end{aligned} \tag{18}$$

To evaluate this term, we have to take the logarithm of the matrix $D_{d,f}^{-1}$. Therefore we split up this matrix into a diagonal part, $D_{d,f,\text{diag}}^{-1}$, and a non-diagonal part, $D_{d,f,\text{non-diag}}^{-1}$. After some algebraic manipulations the logarithm of the remaining non-diagonal term can easily be Taylor expanded. That means one has to split the matrix $D_{d,f}^{-1}$ in the basis (e.g. position space, Fourier space, in the basis of spherical harmonics,...), in which it is mostly dominated by its diagonal:

$$\begin{aligned}
&\ln \left(\frac{1}{2\pi} D_{d,f}^{-1} \right) \\
&= \ln \left(\frac{1}{2\pi} D_{d,f,\text{diag}}^{-1} \right) + \ln \left(1 + D_{d,f,\text{diag}} D_{d,f,\text{non-diag}}^{-1} \right) \\
&= \ln \left(\frac{1}{2\pi} D_{d,f,\text{diag}}^{-1} \right) - \sum_{n=1}^{\infty} \frac{(-1)^n}{n!} \left(D_{d,f,\text{diag}} D_{d,f,\text{non-diag}}^{-1} \right)^n.
\end{aligned} \tag{19}$$

The series expansion can be truncated, if the terms become sufficiently small.

In total, this yields the following expression for the logarithm of the posterior in which f_{nl} -independent constants have been neglected:

$$\begin{aligned}
\ln(P(f|d)) &= -H(f|d) \\
&\approx -\frac{1}{2} \text{tr} \left[\ln \left(\frac{1}{2\pi} D_{d,f,\text{diag}}^{-1} \right) \right] \\
&\quad + \frac{1}{2} \text{tr} \left[\sum_{n=1}^{\infty} \frac{(-1)^n}{n!} \left(D_{d,f,\text{diag}} D_{d,f,\text{non-diag}}^{-1} \right)^n \right] \\
&\quad - H(d, m|f) + \text{const.}
\end{aligned} \tag{20}$$

Thus, we are able to calculate the posterior probability for arbitrary values of f_{nl} under the assumption of a linear response R and additive Gaussian noise n up to some f_{nl} -independent terms and up to the second order in $(\phi - m)$. The very small parameter ϕ justifies the Gaussian approximation of $H(d, \phi|f)$ around its minimum. Thus, Eq. (20) should be a sufficiently precise approximation in order to determine f_{nl} . An example of an f_{nl} -posterior, calculated with this method, is shown in Figure 1 (described in detail in Sec. III.H).

Note that there are no constraints regarding the response, except of its linearity in the primordial gravitational potential, and that the formalism itself is equally valid for correlated noise and for non-constant priors on f_{nl} . The non-linear corrections to the response R arising from the non-linear evolution of primordial perturbations have been shown to be small, $|f_{\text{nl}}| \sim \mathcal{O}(1)$, except for the lensing contributions of the late-time *integrated Sachs-Wolfe effect* (ISW). However, these non-linear contributions can be absorbed in the f_{nl} parameter with the result that the measurement of f_{nl} is non-zero even if the initial f_{nl} is zero [3, 26]. We focus on uncorrelated noise and on a constant f_{nl} -prior for simplicity.

Moreover we are able to calculate the *maximum a posteriori* estimator for f_{nl} , f_{MAP} , analytically by setting $\partial P(f|d)/\partial f|_{f=f_{\text{MAP}}} = 0$. This yields

$$\begin{aligned}
0 &= \frac{1}{2} \text{tr} \left\{ \frac{\partial}{\partial f} \ln \left(\frac{1}{2\pi} D_{d,f}^{-1} \right) \right\} \\
&\quad + \frac{\partial H(d, m|f)}{\partial m} \frac{\partial m}{\partial f} + \frac{\partial H(d, m|f)}{\partial f} \Big|_{f=f_{\text{MAP}}}.
\end{aligned} \tag{21}$$

The exact solution after performing the partial derivatives can be found in Appendix B (Eq. (B1, B2)). Note that we have used the *implicit function theorem* to calculate the partial derivative of the implicitly defined function $m(f)$ with respect to f . Here, too, we do not need any expensive sampling technique to determine f_{MAP} .

III. POSTERIOR VALIDATION AND RESULTS

A. Validation-approach

Now we introduce and apply the DIP-test. This is an appropriate validation method for the f_{nl} -posterior, which is not only able to detect a mistake in the numerical implementation or the mathematical derivation of the posterior but also reveals the kind of an error [19]. For this we use the following procedure [19, 27]:

1. Sample uniformly² a value of f_{gen} from an interval $I = [-f_0, f_0]$, i.e., from a prior

² We assume a uniform prior-distribution for simplicity but this statement is even true for arbitrary distributions.

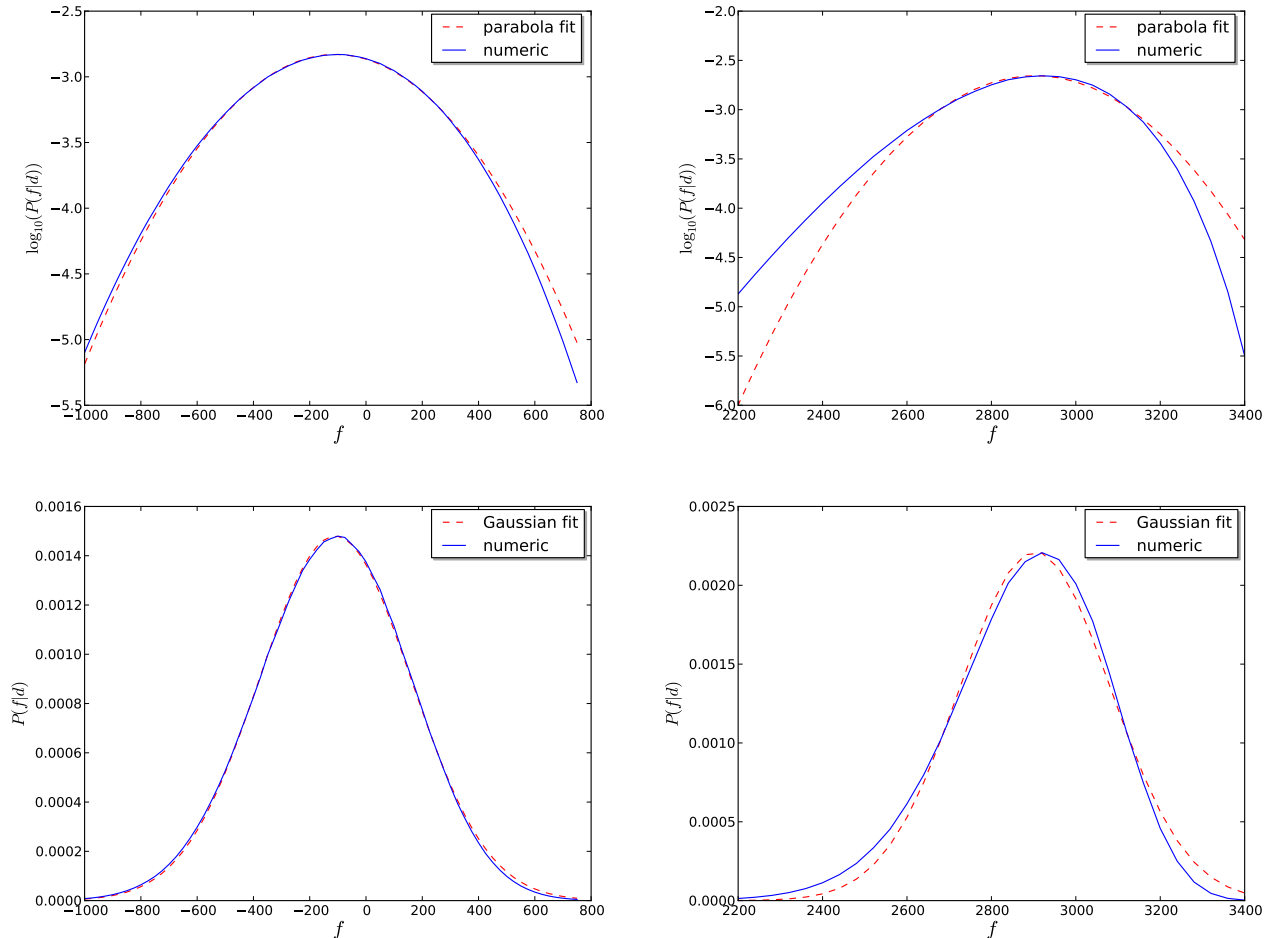


FIG. 1: Normalized posterior distributions for f in a one-dimensional test-case with data generated from $f_{\text{gen}} = 3$ (left) and $f_{\text{gen}} = 3000$ (right). The upper (lower) panels show the numerically calculated posterior including a parabola (Gaussian) fit. For $f_{\text{gen}} = 3000$ the PDF is negatively skewed and thus significantly non-Gaussian. The fitting curves in the upper panels arise from translating the Gaussian fit of the lower panels into a quadratic function.

$$P(f) = \begin{cases} \frac{1}{2f_0} & \text{if } |f| < f_0 \\ 0 & \text{else} \end{cases}. \quad (22)$$

2. Generate data d for f_{gen} according to Eq. (7).
3. Calculate a posterior curve for given data by determining $P(f|d)$ for $f \in I$ according to Eq. (20).
4. Calculate the posterior probability for $f \leq f_{\text{gen}}$ according to

$$x := \int_{-f_0}^{f_{\text{gen}}} df P(f|d) \in [0, 1]. \quad (23)$$

5. If the calculation of the posterior was correct, the distribution for x , $P(x)$, should be uniform between 0 and 1.

We then check the uniformity of $P(x)$ numerically by going through steps 1-4 repeatedly.

B. Power spectrum

The second step of our validation scheme includes the drawing of a Gaussian random field ϕ from its covariance matrix Φ . Considering the Cosmic Microwave Background, we assume statistical homogeneity and isotropy for ϕ , which leads to a diagonal covariance matrix Φ in the basis of spherical harmonics:

$$\Phi_{(lm)(l'm')} = \delta_{ll'} \delta_{mm'} C_l, \quad (24)$$

where $l = 0, 1, \dots, l_{\text{max}}$, $m = -l_{\text{max}}, \dots, l_{\text{max}}$ and C_l is the angular power spectrum of the CMB temperature anisotropies. The value l_{max} is determined by the dis-

cretization of the sphere. C_l is generated with CAMB³ using the cosmological parameters from [1]. In the following, we will consider data on \mathcal{S}^2 as well as one- and two-dimensional flat sky toy-cases.

When considering test cases of a flat data space in one- and two-dimensions, the covariance matrix of the primordial gravitational potential Φ is assumed to be diagonal in the corresponding Fourier space. We set $|k| = l$, where k is a Fourier mode. Hence Φ is given by

$$\Phi_{kk'} = \delta_{kk'} C_k, \quad (25)$$

where $\delta_{kk'}$ is the Kronecker delta symbol and we use the same power spectrum as on the sphere.

C. Flat position space

First we consider one- and two-dimensional tests, for which the primordial gravitational potential is defined over an interval/area on a flat position space, which is discretized into 1024 pixels or, in the case of two dimensions, into 64×64 pixels. For the response and noise covariance matrix we assume the large-scale approximation with $\sigma_n^2 = 1.23 \times 10^{-14}$, given in Eq. (10). The Gaussian random fields ϕ and n were drawn from their covariance matrices Φ and N , respectively. Due to the fact that M is diagonal, we can use Eq. (15) in our numerical implementations. Traces in Eq. (20) are determined by Operator Probing of the NIFTY⁴ package [28] used for calculations throughout this paper.

Figure 2 visualizes the numerical results in the one-dimensional and two-dimensional case. The respective histograms show the unnormalized DIP-distribution of 500 x -values calculated according to Eq. (23). A faulty posterior for f_{nl} would emphasize abundances near to $x = 0$ and $x = 1$ [19, 27], which is not the case. Therefore these uniformly shaped distributions verify the accuracy of our posterior and justify⁵ the saddle point approximation that we have made.

D. One-dimensional position space with Gaussian convolution

In the next test, we leave all specifications made in Sec. C in place but apply a Gaussian convolution with a constant standard deviation of $\sigma = 1.3 \times (\text{distance between the pixels})$ on the field ϕ when generating the data

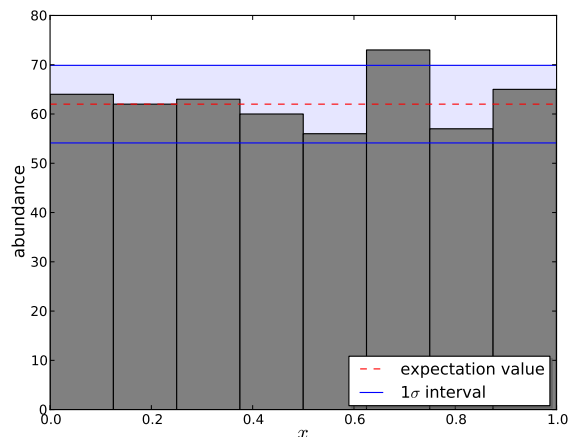
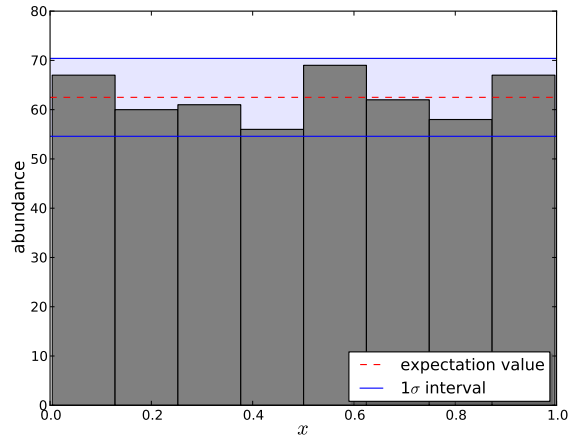


FIG. 2: DIP-distribution of calculated x -values for one- (top) and two-dimensional (bottom) test cases. The histograms show the unnormalized distribution of 500 x -values within eight bins. The standard deviation interval (1σ) around the expectation value as calculated from Poissonian statistics is also shown.

as a part of the response operation. Furthermore we discretize the space into 256 pixels for simplicity. The convolution causes a non-diagonal response matrix and thus a non-diagonal M . Therefore, we have to use the general Eqs. (13), (14) in our numerical implementation.

Figure 3 shows the numerical result. The histogram, showing the unnormalized DIP-distribution of 500 x -values within eight bins, does not emphasize abundances near to $x = 0$ and $x = 1$. Thus, the uniformly shaped distribution again verifies the accuracy of the posterior and justifies our saddle point approximation.

E. Data on the sphere

Finally we consider the primordial gravitational potential on the sphere \mathcal{S}^2 . For the implementation we use the

³ Software to compute the CMB power spectrum; available on http://lambda.gsfc.nasa.gov/toolbox/tb_camb_form.cfm

⁴ <http://www.mpa-garching.mpg.de/ift/nifty/>

⁵ Note that there is an unlikely possibility of at least two errors compensating each other precisely. If so, the distribution of x would be uniform, albeit an error in the implementation or mathematical derivation of the posterior.

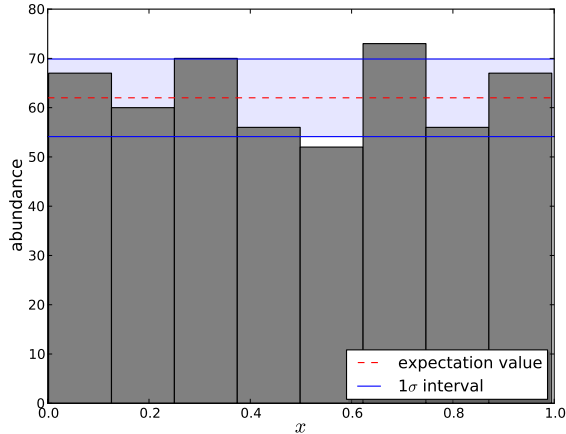


FIG. 3: DIP-distribution of calculated x -values for the one-dimensional test case with Gaussian convolution. The histogram shows the unnormalized distribution of 500 x -values within eight bins. The standard deviation interval (1σ) around the expectation value as calculated from Poissonian statistics is also shown.

HEALPix⁶ package to discretize the sphere into $12N_{\text{side}}^2$ pixels. We still use the large-scale approximation with $\sigma_n^2 = 1.23 \times 10^{-14}$ and $N_{\text{side}} = 32$.

Figure 4 visualizes the numerical result. The histogram shows again the unnormalized DIP-distribution of 500 x -values within eight bins. In marked contrast to the flat space test cases abundances near to $x = 0$ and $x = 1$ are highly emphasized, which indicates an insufficient posterior. The convex “U-shape” of the distribution indicates an underestimation ($\approx 35\%$) of the standard deviation σ_f of our numerical implementation of the posterior with respect to the correct f_{nl} -posterior (see DIP-test, [19], for details). Due to the fact that we changed only the basis of the space in comparison to the Cartesian tests (see III.C, III.D), the test failure and thus the underestimation of the standard deviation is likely due to the insufficient precision of the numerical transformations between the basis of spherical harmonics and the HEALPix-space and thus numerical in nature.

F. Reconstruction of the primordial gravitational potential

Up to now we have focused on the accuracy of the f_{nl} -posterior. However, we are also able to reconstruct the primordial gravitational potential φ or the auxiliary Gaussian field ϕ from the data d . For this we assume the minimum of the Hamiltonian up to quadratic order in f (see Eq. (8), (9), (13)) to be a precise estimate for ϕ . φ

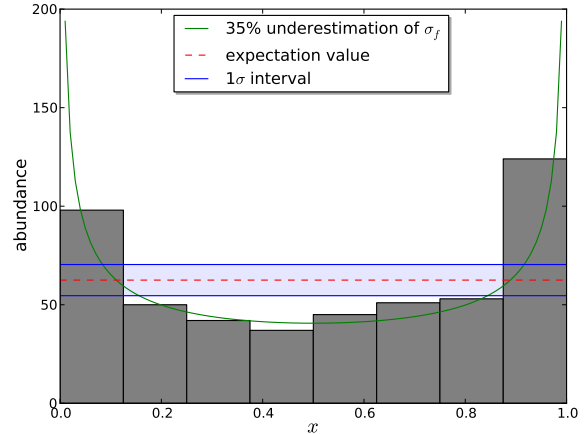


FIG. 4: DIP-distribution of calculated x -values for the test case on the sphere. The histogram shows the unnormalized distribution of 500 x -values within eight bins. The standard deviation interval (1σ) around the expectation value as calculated from Poissonian statistics is also shown. The green curve shows the analytical shape of a Gaussian posterior-distribution whose standard deviation deviates by 35% from the one of the true Gaussian posterior.

is reconstructed by applying a *Wiener Filter* [29] on the data, given by

$$m_w = (\Phi^{-1} + R^\dagger N^{-1} R)^{-1} R^\dagger N^{-1} d = D j. \quad (26)$$

Fig. 5 shows an example of this reconstruction, where we have used the specifications made in Sec. D with $N_{\text{side}} = 32$, $f_{\text{nl}} = 2000$, and $\sigma_n^2 = 0.5 \times 10^{-11}$. We have chosen this large value of f_{nl} and σ_n^2 to demonstrate the reconstruction at a high level of non-Gaussianity and noise.

G. Comparison to the KSW-estimator for f_{nl}

A common procedure to determine the level of non-Gaussianity is the application of the *KSW*-estimator developed in [12] for f_{nl} , which uses the CMB-bispectrum and is given by [12, 17]

$$\hat{f}_{KSW} = \frac{1}{\mathcal{N}} m_w^\dagger \Phi^{-1} m_w^2 \quad (27)$$

with the data-independent normalization constant

$$\mathcal{N} = \langle m_w^\dagger \Phi^{-1} m_w^2 \rangle_{(d,s|f=1)} \quad (28)$$

and the standard deviation $\sigma_{\hat{f}_{KSW}} = 1/\sqrt{\mathcal{N}}$. This means the PDF for f_{nl} is Gaussian, given by $\mathcal{G}(\hat{f}_{KSW}, \sigma_{\hat{f}_{KSW}}^2)$.

⁶ <http://healpix.jpl.nasa.gov/>

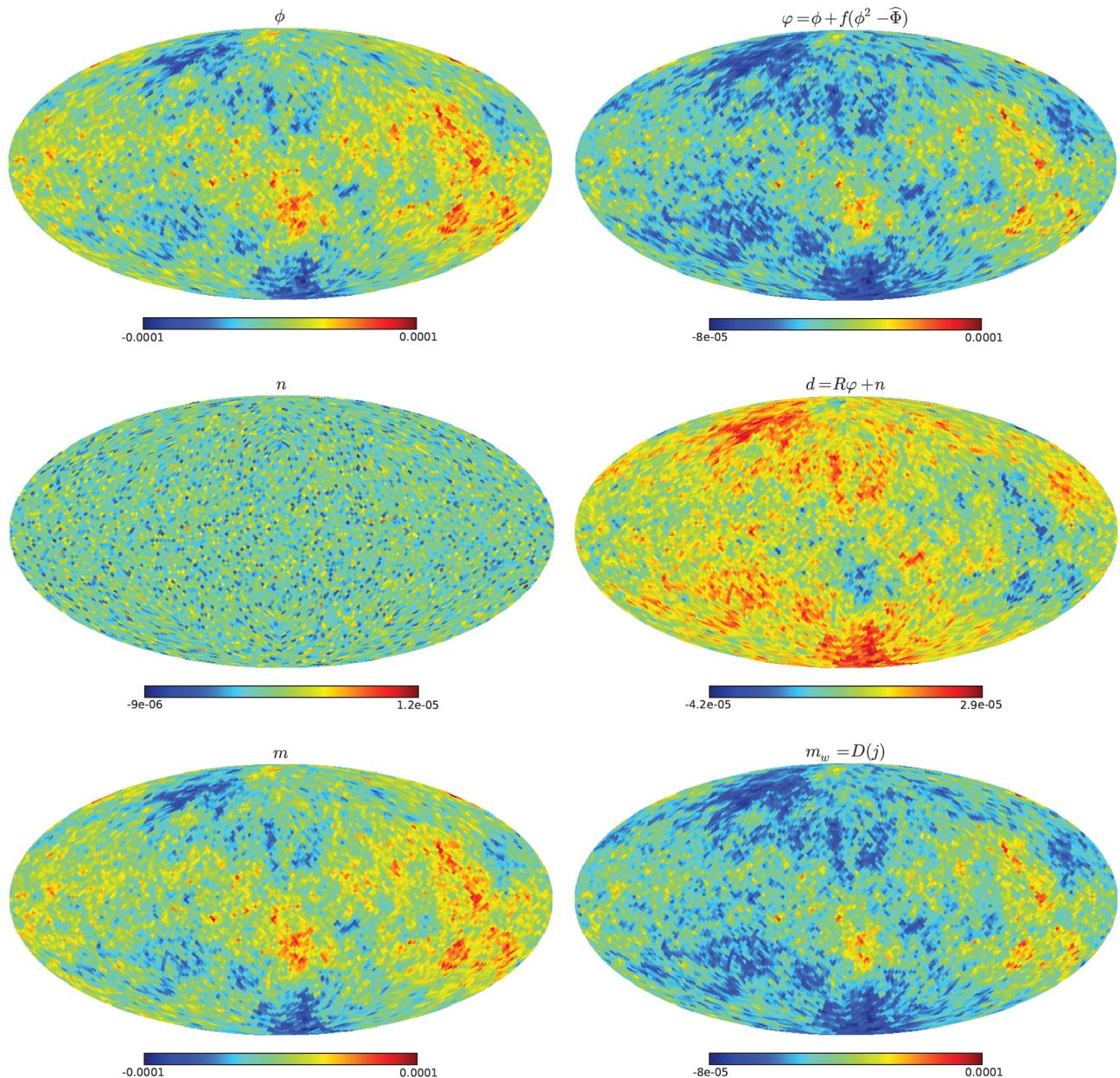


FIG. 5: Reconstruction of the primordial gravitational potential φ or the auxiliary Gaussian field ϕ by using the maximum of the Hamiltonian and by applying a *Wiener Filter*, respectively. The upper four panels are showing the generation of the mock data d , whereas the last two panels are showing the reconstructions of the original fields. Note the different color codes.

Note that the standard deviation $\sigma_{\hat{f}_{KSW}}$ can also be obtained by sampling the PDF of the *KSW*-estimator and reading off its value.

The first difference in comparison to our posterior is the reduction of a PDF to a single number and as a consequence thereof a large loss of information. In particular this becomes problematic if the PDF is not symmetric around the estimated value. The second difference is the data-independence of the uncertainty, determined by averaging over data and signal realizations, given a unit f_{nl} .

To visualize the influence of these effects on the accuracy of the *KSW*-estimator, we apply the DIP-test to the latter with the numerical settings made in III.C for the one-dimensional case, but use $\sigma_n^2 = 10^{-15}$, and a white power spectrum in position space, $\sigma_\phi^2 = 10^{-10}$. We perform the DIP-test within the intervals $I_1 = [-6000, 6000]$ and $I_2 = [-2000, 2000]$. The normalization \mathcal{N} is calculated from 1.06×10^8 data realizations. The results are shown in Fig. 6.

The characteristic and significant “U”-shape of the left and middle DIP-distribution in Fig. 6 encodes an under-

estimation of the standard deviation $\sigma_{\hat{f}_{KSW}}$ on average (for details see [19]), whereas for our posterior we obtain a flat distribution. The underestimation arises from the wrong assumption of symmetric errors with respect to \hat{f}_{KSW} for large values of the underlying, true value of f_{nl} . However, with a decreasing value of f_{nl} the distribution becomes flatter and will be uniform in the limit of small values of f_{nl} .

Another difference between the estimator and our posterior is the computational costs. In marked contrast to the *KSW*-estimator we do not need a numerically expensive sampling technique to determine the normalization because we got rid of the ϕ -marginalization by replacing the exact Hamiltonian by its Taylor expansion and performing the ϕ -integration afterwards (see II.B).

H. Shape of the f_{nl} -posterior

In order to investigate the shape of the f_{nl} -posterior we consider the one-dimensional test case presented in III.C. In agreement with results concerning f_{nl} -estimators, e.g. [14], our posterior can deviate from a Gaussian. While for $f_{nl} \approx 0$ the PDF is approximately Gaussian, for $f_{nl} \gg 0$ it is negatively skewed and for $f_{nl} \ll 0$ it is positively skewed. The deviations for $f_{nl} \neq 0$ arise mainly from the determinant-part of Eq. (20) and increase with the value of f_{nl} . Fig. 1 illustrates this effect. The small deviations for $f_{nl} = 3$ do not emerge due to a non-vanishing f_{nl} , but arise during the generation of the Gaussian random field ϕ , which contains tiny correlations between small and large scales. However, the PDF for $f_{nl} = 3$ is Gaussian on average. Although the deviations from a Gaussian can be neglected in practice for realistic values of f_{nl} , constrained recently by the *Planck* Collaboration to be $f_{nl} = 2.7 \pm 5.8$ (68% CL statistical) [3], we want to stress that the general approach of non-Gaussianity estimation and posterior verification can be applied to other forms of non-Gaussianity as well.

Note that in contrast to the negatively skewed posterior the estimator for f_{nl} of [14] is positively skewed. The reason for the apparently inconsistency is that we use $R = -1/3$ instead of a unit response .

IV. THE BAYESIAN g_{nl} -POSTERIOR

Until now we have focused on first order deviations from Gaussianity (i.e. deviations from Gaussianity are dominated by the bispectrum), which are characterized by the f_{nl} -parameter. Now we want to extend our formalism to higher order deviations. The next leading order is described by the trispectrum, which can be parametrized by the so-called g_{nl} -parameter. If we take g_{nl} into account the primordial gravitational potential reads [18]

$$\tilde{\varphi} = \phi + f_{nl} \left(\phi^2 - \hat{\Phi} \right) + g_{nl} \left(\phi^3 - 3\phi \star \hat{\Phi} \right). \quad (29)$$

One has to consider this order, for instance, if deviations from Gaussianity are significantly influenced by the trispectrum or even dominated by it. Here we consider the latter, i.e. $f_{nl} \approx 0$, to avoid too lengthy formulas. Thus, the data are given by

$$d = R \left(\phi + g_{nl} \left(\phi^3 - 3\phi \star \hat{\Phi} \right) \right) + n, \quad (30)$$

and the information Hamiltonian by

$$H(d, \phi|g) = H_0 + \frac{1}{2} \phi^\dagger D^{-1} \phi - j^\dagger \phi + \sum_{n=0}^6 \frac{1}{n!} \Omega^{(n)}[\phi, \dots, \phi], \quad (31)$$

with the additional (in comparison to Sec. II) abbreviations

$$\begin{aligned} g &= g_{nl}, \quad \Omega^{(0)} = 0 = \Omega_{xyzuv}^{(5)} \\ \Omega_x^{(1)} &= 3g_x \hat{\Phi}_x j_x, \\ \Omega_{xy}^{(2)} &= \left(\frac{9}{2} g_x \hat{\Phi}_x M_{xy} g_y \hat{\Phi}_y - 3M_{xy} g_y \hat{\Phi}_y \right. \\ &\quad \left. + 1 \text{ perturbation} \right), \\ \Omega_{xyz}^{(3)} &= \left(- (gj)_x \delta_{xy} \delta_{xz} + 5 \text{ perturbations} \right), \\ \Omega_{xyzuv}^{(4)} &= \left(M_{xy} g_y \delta_{yz} \delta_{yu} - 3g_x M_{xy} g_y \hat{\Phi}_y \delta_{yz} \delta_{yu} \right. \\ &\quad \left. + 23 \text{ perturbations} \right), \\ \Omega_{xyzuvw}^{(6)} &= \left(\frac{1}{2} \delta_{xy} \delta_{zy} g_y M_{yu} g_u \delta_{uv} \delta_{uw} \right. \\ &\quad \left. + 719 \text{ perturbations} \right). \end{aligned} \quad (32)$$

Now we are able to perform again a saddle-point-approximation in the primordial gravitational potential around the minimum of $H(d, \phi|g)$. The minimum \tilde{m} and the Hessian $D_{d,g}^{-1}$ of the Hamiltonian are given by

$$\begin{aligned} 0 &= \left(D^{-1} + \Omega^{(2)} \right) \tilde{m} - j + \left(\Omega^{(1)} \right)^\dagger \\ &\quad - 3gj \star \tilde{m}^2 + 3g \left(\frac{1}{3} M \tilde{m}^3 + \tilde{m}^2 \star M \tilde{m} - gM \left(\hat{\Phi} \star \tilde{m}^3 \right) \right. \\ &\quad \left. - 3g \left(\hat{\Phi} \star \tilde{m}^2 \right) \star M \tilde{m} \right) + 3g^2 \tilde{m}^2 \star M \tilde{m}^3, \end{aligned} \quad (33)$$

and

$$\begin{aligned} \left(D_{d,g}^{-1} \right)_{xy} &= D_{xy}^{-1} + \Omega_{xy}^{(2)} - 6g j_x \tilde{m}_x \delta_{xy} + 6g \left(M_{xy} \tilde{m}_y^2 \right. \\ &\quad \left. + \tilde{m}_x (M \tilde{m})_x \delta_{xy} - 3g (M_{xy} \hat{\Phi}_y \tilde{m}_y^2 + \hat{\Phi}_x \tilde{m}_x (M \tilde{m})_x \delta_{xy}) \right) \\ &\quad + 6g^2 \left(\tilde{m}_x (M \tilde{m}^3)_x \delta_{xy} + \frac{3}{2} \tilde{m}_x^2 M_{xy} \tilde{m}_y^2 \right), \end{aligned} \quad (34)$$

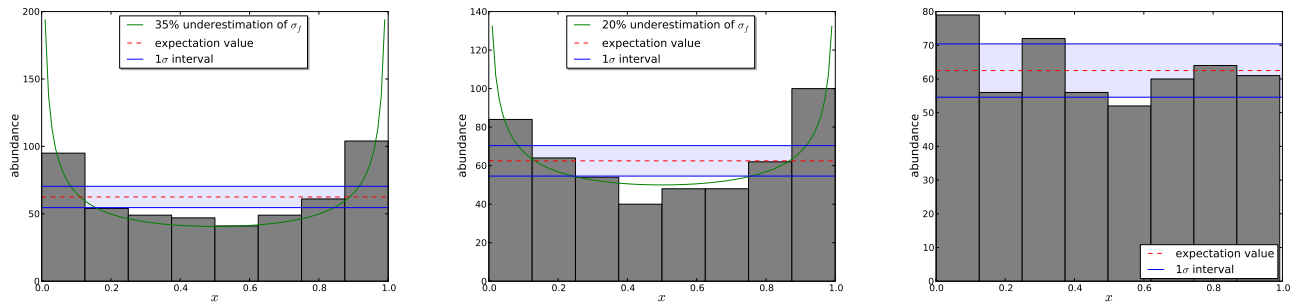


FIG. 6: DIP-distributions of calculated x -values for the KSW -estimator (left, middle) and approximated posterior according to Eq. (20) (right) and according to the intervals $I_1 = [-6000, 6000] \ni f_{\text{nl}}$ (left, right), $I_2 = [-2000, 2000] \ni f_{\text{nl}}$ (middle). The histograms show the unnormalized distributions of 500 x -values within eight bins. The standard deviation interval (1σ) around the expectation value as calculated from Poissonian statistics is also shown. The green line in the left (middle) panel is a theoretical DIP-distribution calculated with a Gaussian posterior, whose standard deviation was underestimated by 35% (20%).

if we assume g_{nl} to be a scalar⁷. Thus, the posterior for g_{nl} can be calculated as follows:

$$\begin{aligned}
 \ln(P(g|d)) &= -H(g|d) \\
 &= -\frac{1}{2} \text{tr} \left[\ln \left(\frac{1}{2\pi} D_{d,g,\text{diag}}^{-1} \right) \right] \\
 &\quad + \frac{1}{2} \text{tr} \left[\sum_{n=1}^{\infty} \frac{(-1)^n}{n!} \left(D_{d,g,\text{diag}} D_{d,g,\text{non-diag}}^{-1} \right)^n \right] \\
 &\quad - H(d, \tilde{m}|g) + \text{const.}
 \end{aligned} \tag{35}$$

Analogous to Eq. (20) the series expansion can be truncated if the terms become sufficiently small.

Note that our formalism does not require a value of $f_{\text{nl}} \approx 0$. One can easily include $f_{\text{nl}}, g_{\text{nl}}$ and even higher order corrections into the Hamiltonian and is still able to do the stated Taylor expansion due to the fact that the expansion parameter is ϕ and not f_{nl} or g_{nl} .

V. CONCLUDING REMARKS

We derived a precise probability density function for the non-Gaussianity parameter f_{nl} in the framework of information field theory. For this we considered temperature anisotropies of the Cosmic Microwave Background. During this calculation we used a saddle point approximation by performing a Taylor expansion around the minimum of the so-called information Hamiltonian (see ((13), (14)) and assumed a linear response of the data to the primordial gravitational potential φ , Gaussian noise,

and an f_{nl} -independent prior, $P(f)$. The precision of the posterior was validated by the DIP-test (see Sec. III.A and [19, 27]).

In the application examples concerning a flat sky (see III.C and III.D) we have verified the precision of the derived posterior, whereas in the test case on the sphere (see III.E) we have shown its numerical insufficiency. One likely reason for this failure is the insufficient precision of the numerical transformations between the basis of spherical harmonics and the HEALPix-space, since the basis transformations are the only qualitative difference between the failed spherical test and the successful Cartesian tests. As a consequence of this, it would be necessary to investigate the numerical precision of the basis transformations on the sphere [30, 31] in order to ensure that published f_{nl} -estimators [3] are not affected by this.

A comparison to the KSW -estimator (see III.G) revealed a precise performance of the derived f_{nl} -posterior even for high values of f_{nl} , while the uncertainty estimate for the KSW -estimator is becoming worse with an increasing (high) value of f_{nl} .

Furthermore we have presented a well working non-linear reconstruction method for the primordial gravitational field φ on the sphere \mathcal{S}^2 (see Sec. III.F) and have investigated the shape of the f_{nl} -posterior (see III.H), which is negatively (positively) skewed for $f_{\text{nl}} \gg 0$ ($f_{\text{nl}} \ll 0$) and Gaussian for $f_{\text{nl}} \approx 0$ (e.g. [14]).

Note that by including a Gaussian convolution in the response on the primordial gravitational field we have shown that more complex cases than the Sachs-Wolfe limit of local response can be dealt with. Therefore, the presented method should also be applicable to *Planck* CMB maps at full resolution when efficient and accurate transformations (for instance between the three-dimensional position space) are used [15].

Finally we have extended our formalism to the next leading order of non-Gaussianity, which can be parametrized by g_{nl} , in Sec. IV and have explained how to even go beyond this.

⁷ Note that Eqs. (31), (32) allow to consider a spatially varying g_{nl} , too. We focus on a scalar for simplicity.

Acknowledgments

We want to thank Henrik Junklewitz and Maksim Greiner for useful discussions. The results in III.E have been derived using the HEALPix package [32]. Calculations were realized using the NIFTY [28] package.

Appendix A: Functional derivatives of the Hamiltonian

Equations (13) and (14) are based on:

$$\begin{aligned}
& \frac{\delta}{\delta\phi(w)} \Lambda^{(3)}[\phi, \phi, \phi] \\
&= 6f \frac{\delta}{\delta\phi(w)} \int dx \int dy \int dz \phi(y) M(y, x) \\
&\quad \times \delta(x-z) \phi(x) \phi(z) \\
&= 6f \frac{\delta}{\delta\phi(w)} \int dx \int dy \phi(y) M(y, x) \phi^2(x) \\
&= 6f \int dx \int dy \delta(y-w) M(y, x) \phi^2(x) \\
&\quad + 12f \int dx \int dy \phi(y) M(y, x) \phi(x) \delta(w-x) \\
&= (6fM\phi^2 + 12f\phi \star M\phi)(w)
\end{aligned} \tag{A1}$$

$$\begin{aligned}
& \frac{\delta^2}{\delta\phi(w)\delta\phi(v)} \Lambda^{(3)}[\phi, \phi, \phi] \\
&= 6(2f \int dx M(w, x) \phi(x) \delta(x-v) \\
&\quad + 2f \int dy \phi(w) M(w, y) \delta(y-v) \\
&\quad + 2f \int dy \phi(y) M(y, w) \delta(w-v)) \\
&= (6(4f\phi \star M + 2f\widehat{M\phi})) (w, v)
\end{aligned} \tag{A2}$$

$$\begin{aligned}
& \frac{\delta}{\delta\phi(w)} \Lambda^{(4)}[\phi, \phi, \phi, \phi] \\
&= 24 \left(\frac{f^2}{2} \frac{\delta}{\delta\phi(w)} \int dx \int dv \phi^2(x) M(x, v) \phi^2(v) \right) \\
&= 24(f^2 \int dv \phi(w) M(w, v) \phi(v)^2 \\
&\quad + f^2 \int dx \phi(x)^2 M(x, w) \phi(w)) \\
&= (48f^2\phi \star M\phi^2)(w)
\end{aligned} \tag{A3}$$

$$\begin{aligned}
& \frac{\delta^2}{\delta\phi(w)\delta\phi(v)} \Lambda^{(4)}[\phi, \phi, \phi, \phi] \\
&= 24(4f^2 \int dx \phi(w) M(w, x) \phi(x) \delta(x-v) \\
&\quad + 2f^2 \int dx \delta(w-v) M(w, x) \phi^2(x)) \\
&= (24(4f^2\phi^2 \star M + 2f^2\widehat{M\phi^2}))(w, v)
\end{aligned} \tag{A4}$$

Appendix B: Analytic solution of the MAP-estimator for f_{nl}

Performing the partial derivatives of Eq. (21) yields

$$\begin{aligned}
& \frac{1}{2} \text{tr} \left\{ D_{d,f} (\Lambda_f^{(2)} + fm \star M + 2\widehat{Mm} + 8fm^2 \star M \right. \\
&\quad \left. + 4f\widehat{Mm^2}) \right\} - \left\{ (D^{-1} + \Lambda^{(2)}) m - j + \Lambda^{(1)} \right. \\
&\quad \left. + fMm^2 + 2fm \star Mm + 2f^2m \star Mm^2 \right\}^\dagger D_{d,f} \\
&\quad \times \left\{ Mm^2 + 2m \star Mm + 4fm \star Mm^2 \right\} \\
&\quad + \sum_{n=0}^4 \frac{1}{n!} \Lambda_f^{(n)}[\phi, \dots, \phi] = 0,
\end{aligned} \tag{B1}$$

with the abbreviations

$$\begin{aligned}
\Lambda_f^{(0)} &= j^\dagger \widehat{\Phi} + f\widehat{\Phi}^\dagger M\widehat{\Phi}, \\
\Lambda_f^{(1)} &= -\widehat{\Phi}^\dagger M, \\
\Lambda_f^{(2)} &= -2\widehat{j}, \\
(\Lambda_f^{(3)})_{xyz} &= (M_{xy}\delta_{yz} + 5 \text{ perturbations}), \\
(\Lambda_f^{(4)})_{xyzu} &= (f_x\delta_{xy}M_{yz}\delta_{zu} + 23 \text{ perturbations}).
\end{aligned} \tag{B2}$$

-
- [1] C. L. Bennett, D. Larson, J. L. Weiland, N. Jarosik, G. Hinshaw, N. Odegard, K. M. Smith, R. S. Hill, B. Gold, M. Halpern, et al., ArXiv e-prints (2012), 1212.5225.
- [2] Planck Collaboration, P. A. R. Ade, N. Aghanim, C. Armitage-Caplan, M. Arnaud, M. Ashdown, F. Atrio-Barandela, J. Aumont, C. Baccigalupi, A. J. Banday, et al., ArXiv e-prints (2013), 1303.5076.
- [3] Planck Collaboration, P. A. R. Ade, N. Aghanim, C. Armitage-Caplan, M. Arnaud, M. Ashdown, F. Atrio-Barandela, J. Aumont, C. Baccigalupi, A. J. Banday, et al., ArXiv e-prints (2013), 1303.5084.
- [4] N. Bartolo, E. Komatsu, S. Matarrese, and A. Riotto, Physical Reports **402**, 103 (2004), arXiv:astro-ph/0406398.
- [5] T. Falk, R. Rangarajan, and M. Srednicki, ApJL **403**, L1 (1993), arXiv:astro-ph/9208001.
- [6] A. Gangui, Phys. Rev. D **50**, 3684 (1994), arXiv:astro-ph/9406014.
- [7] D. S. Salopek and J. R. Bond, Phys. Rev. D **42**, 3936 (1990).
- [8] P. J. E. Peebles, Astrophys. J. **510**, 523 (1999), arXiv:astro-ph/9805194.
- [9] E. Komatsu and D. N. Spergel, Phys. Rev. D **63**, 063002 (2001), arXiv:astro-ph/0005036.
- [10] J. M. Bardeen, P. J. Steinhardt, and M. S. Turner, Phys. Rev. D **28**, 679 (1983).
- [11] E. Komatsu, ArXiv Astrophysics e-prints (2002), arXiv:astro-ph/0206039.
- [12] E. Komatsu, D. N. Spergel, and B. D. Wandelt, Astrophys. J. **634**, 14 (2005), arXiv:astro-ph/0305189.
- [13] P. Creminelli, L. Senatore, and M. Zaldarriaga, Journal of Cosmology and Astro-Particle Physics **3**, 019 (2007), arXiv:astro-ph/0606001.
- [14] T. L. Smith, M. Kamionkowski, and B. D. Wandelt, Phys. Rev. D **84**, 063013 (2011), 1104.0930.
- [15] F. Elsner and B. D. Wandelt, Astrophys. J. **724**, 1262 (2010), 1010.1254.
- [16] F. Elsner, B. D. Wandelt, and M. D. Schneider, Astronomy and Astrophysics **513**, A59 (2010), 1002.1713.
- [17] T. A. Enßlin, M. Frommert, and F. S. Kitaura, Phys. Rev. D **80**, 105005 (2009), 0806.3474.
- [18] L. Verde, R. Jimenez, L. Alvarez-Gaume, A. F. Heavens, and S. Matarrese, Journal of Cosmology and Astro-Particle Physics **6**, 023 (2013), 1301.6017.
- [19] S. Dorn, N. Opperman, and T. A. Enßlin, ArXiv e-prints (2013).
- [20] R. K. Sachs and A. M. Wolfe, Astrophys. J. **147**, 73 (1967).
- [21] M. White and W. Hu, Astronomy and Astrophysics **321**, 8 (1997), arXiv:astro-ph/9609105.
- [22] T. Bayes, Phil. Trans. of the Roy. Soc. **53**, 370 (1763).
- [23] U. Seljak and M. Zaldarriaga, Astrophys. J. **469**, 437 (1996), arXiv:astro-ph/9603033.
- [24] A. Lewis, A. Challinor, and A. Lasenby, Astrophys. J. **538**, 473 (2000), arXiv:astro-ph/9911177.
- [25] M. Doran, Journal of Cosmology and Astro-Particle Physics **10**, 011 (2005), arXiv:astro-ph/0302138.
- [26] D. M. Goldberg and D. N. Spergel, Phys. Rev. D **59**, 103002 (1999), arXiv:astro-ph/9811251.
- [27] S. R. Cook, A. Gelman, and D. B. Rubin, Journal of Computational and Graphical Statistics **15**, 675 (2006).
- [28] M. Selig, M. R. Bell, H. Junklewitz, N. Oppermann, M. Reinecke, M. Greiner, C. Pachajoa, and T. A. Enßlin, Astronomy and Astrophysics **554**, A26 (2013), 1301.4499.
- [29] N. Wiener, *Extrapolation, Interpolation, and Smoothing of Stationary Time Series* (New York: Wiley, 1949), ISBN 9780262730051.
- [30] M. Reinecke, Astronomy and Astrophysics **526**, A108 (2011), 1010.2084.
- [31] M. Reinecke and D. Sverre Seljebotn, ArXiv e-prints (2013), 1303.4945.
- [32] K. M. Górski, E. Hivon, A. J. Banday, B. D. Wandelt, F. K. Hansen, M. Reinecke, and M. Bartelmann, The Astrophysical Journal **622**, 759 (2005).